INTERFACE

rsif.royalsocietypublishing.org

Research

Cite this article: Kariko S, Timonen JVI, Weaver JC, Gur D, Marks C, Leiserowitz L, Kolle M, Li L. 2018 Structural origins of coloration in the spider *Phoroncidia rubroargentea* Berland, 1913 (Araneae: Theridiidae) from Madagascar. *J. R. Soc. Interface* **15**: 20170930.
http://dx.doi.org/10.1098/rsif.2017.0930

Received: 11 December 2017
Accepted: 30 January 2018

Subject Category:
Life Sciences–Physics interface

Subject Areas:
biomaterials, nanotechnology

Keywords:
spider, structural colour, guanine, *Phoroncidia*

Authors for correspondence:
Sarah Kariko
e-mail: sjkariko@gmail.com
Ling Li
e-mail: lingl@vt.edu

Electronic supplementary material is available online at https://dx.doi.org/10.6084/m9.figshare.c.3999489.

THE ROYAL SOCIETY PUBLISHING

Structural origins of coloration in the spider *Phoroncidia rubroargentea* Berland, 1913 (Araneae: Theridiidae) from Madagascar

Sarah Kariko[1], Jaakko V. I. Timonen[2,5], James C. Weaver[3], Dvir Gur[6], Carolyn Marks[4], Leslie Leiserowitz[7], Mathias Kolle[8] and Ling Li[9]

[1]Museum of Comparative Zoology, [2]Harvard John A. Paulson School of Engineering and Applied Sciences, [3]Wyss Institute for Biologically Inspired Technology, and [4]Center for Nano Sciences, Harvard University, Cambridge, MA 02138, USA
[5]Department of Applied Physics, Aalto University School of Science, Espoo 02150, Finland
[6]Department of Physics of Complex Systems and Department of Molecular Cell Biology, and [7]Department of Materials and Interfaces, Weizmann Institute of Science, Rehovot 76100, Israel
[8]Department of Mechanical Engineering, Massachusetts Institute of Technology, Cambridge, MA 02139, USA
[9]Department of Mechanical Engineering, Virginia Tech, Blacksburg, VA 24060, USA

LL, 0000-0002-6741-9741

This study investigates the structural basis for the red, silver and black coloration of the theridiid spider, *Phoroncidia rubroargentea* (Berland, 1913) from Madagascar. Specimens of this species can retain their colour after storage in ethanol for decades, whereas most other brightly pigmented spider specimens fade under identical preservation conditions. Using correlative optical, structural and chemical analysis, we identify the colour-generating structural elements and characterize their optical properties. The prominent silvery appearance of the spider's abdomen results from regularly arranged guanine microplatelets, similar to those found in other spiders and fish. The microplatelets are composed of a doublet structure twinned about the $[02\bar{1}]$ axis, as suggested by electron diffraction. The red coloration originates from chambered microspheres (approx. 1 µm in diameter), which contain structured fluorescent material. Co-localization of the red microparticles on top of the reflective guanine microplatelets appears to enhance the red coloration. The spider's thick cuticular layer, which encases its abdomen, varies in its optical properties, being transparent in regions where only guanine reflectors are present, and tanned, exhibiting light absorption where the red microspheres are found. Moreover, colour degradation in some preserved spider specimens that had suffered damage to the cuticular layer suggests that this region of the exoskeleton may play an important role in the stabilization of the red coloration.

1. Introduction

Since Hooke and Newton in the seventeenth century, scientists have been investigating the material structures and mechanisms creating the breathtaking spectrum of colours in Nature [1,2]. Typically, the focus has been on the colourful feathers of birds, including peacocks and birds-of-paradise [3,4], the iridescent elytra of beetles [5], and the brightly coloured wings of butterflies [6–8]. Recently, however, arachnids, especially spiders, have received increasing attention in terms of structural coloration [9–12]. Some spiders are vividly coloured and patterned by utilizing a variety of coloration strategies and some species even display the capacity for dynamic colour change [13–18], providing intriguing models for investigating colour production in nature. Understanding the phenomena underlying structurally enhanced

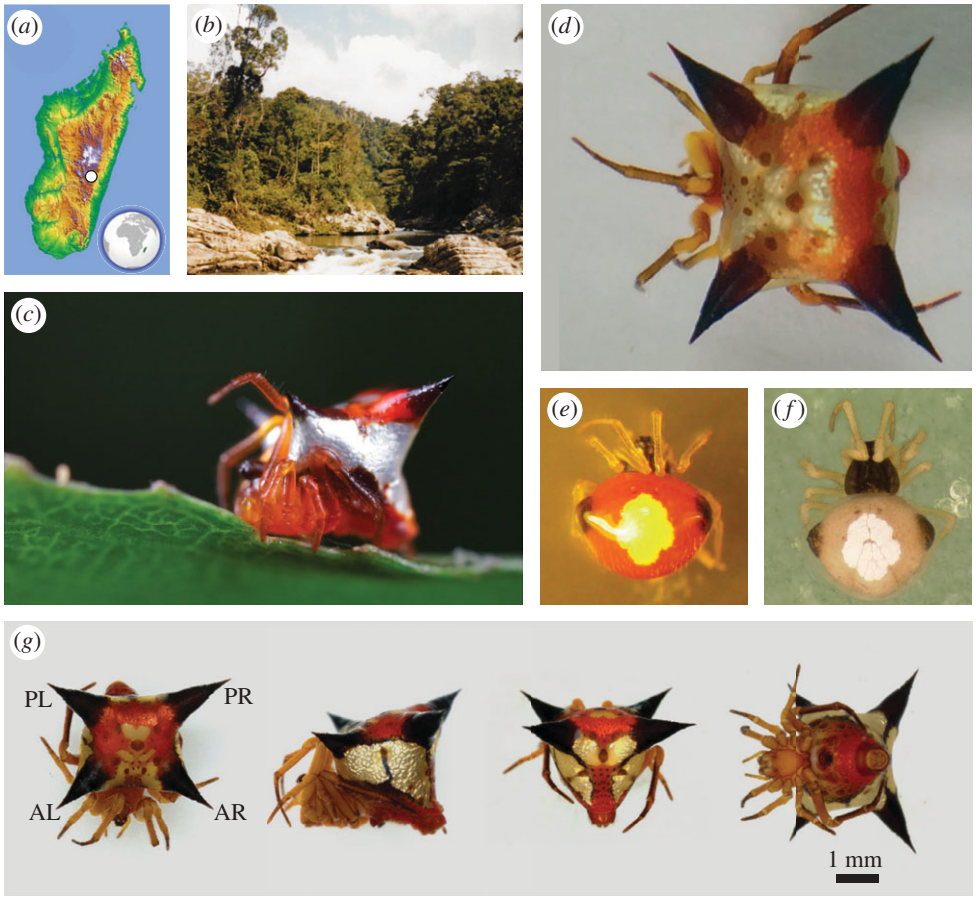

Figure 1. Information of distribution, habitat and overall appearance of *P. rubroargentea* (Berland, 1913). (*a*) Map of Madagascar. The white dot indicates the location of Ranomafana National Park. (*b*) Photo of the rainforest in Ranomafana National Park where *P. rubroargentea* have been found. (*c*) Photo of a live *Phoroncidia* in the field (credit: Paul Bertner). (*d*) *P. rubroargentea* stored in ethanol for 40 years (14 600 days), which still retains the vibrant red colour (MCZ IZ 32022). *Theridula emertoni* (MCZ IZ 143122) (*e*) before and (*f*) after 220 days in 70% ethanol. (*g*) Multiple views of a *P. rubroargentea* examined in this study (CASENT 9057540): PL, posterior left; PR, posterior right; AL, anterior left; AR, anterior right.

coloration in spiders can potentially provide new design cues for the design of photonic devices [11,19] and offer insights into the biological function of such colours.

Currently, it is known that spiders use multiple coloration strategies (structural colour, pigmentation and fluorescence) for visual display, similar to those implemented by other animal groups. Structural colour is produced from the interaction of light with nano- and microstructures, which results in the spectrally selective reflection or scattering of light. One of the most common optical displays in spiders that relies on this light interaction with nano/microscopic structures is the silvery reflection or matt white appearance originated from guanine crystals [12,20–22]. Similar to other groups (e.g. fishes, reptiles and other arthropods), spiders have evolved a mechanism in which guanine is diverted from the digestive tract and stored in specialized cells called guanocytes under the cuticle of the abdomen, where they scatter and reflect light [20–23]. A matte white appearance results from prismatic-shaped guanine crystals, which can provide a canvas-like background for pigment-based colour [22]. By contrast, a silvery and specularly reflecting surface appearance originates from microscopic platelet-shaped guanine crystals [12,20–22]. Spiders with a guanine-based silvery appearance are widespread across different families, ranging from tiny dewdrop spiders in the genus *Argyrodes* (family: Theridiidae) such as *Argyrodes elevatus* Taczanowski, 1873, to long jawed spiders in the family Tetragnathidae, such as *Tetragnatha montana* Simon, 1874 [21,22]. Spiders with structural colour originating from structures other than from guanine-based reflectors are found in a few families, such as Theraphosidae (tarantulas) and Salticidae (jumping spiders) [9,24].

In addition to structural coloration, spiders also use pigments to create colours through the selective absorption of specific wavelengths of incident light. There are six common classes of biochromes (biological pigments) used to produce colours in animals: melanins, carotenoids, ommochromes, bilins, porphyrines and pterins [10,25]. Of these, ommochromes, melanins and bilins have been found in spiders [10,15,26–28], whereas the presence of porphryines, carotenoids and pterins in spiders has not yet been established [12,28]. Ommochromes are the primary biological pigment present in spiders and are responsible for the yellows, reds, oranges, browns and blacks [15,29]. While melanin, which is responsible for many of the dark colours from reddish brown to black [30], was only recently detected in spiders by Hsiung *et al*. [31], further study is needed to understand how widely distributed this pigment is across spider taxa [31]. Billins are a class of green pigments that have also been found in some spiders and are usually either concentrated in the exoskeleton or are present in the haemolymph (blood) and visible through transparent cuticles [26,32]. The carotenoid pigment class is usually associated with creating colours ranging from dark red to pale yellow, however these pigments are acquired through consuming plants or herbivores, and among arachnids they have so far only been found in some mites [12,33,34].

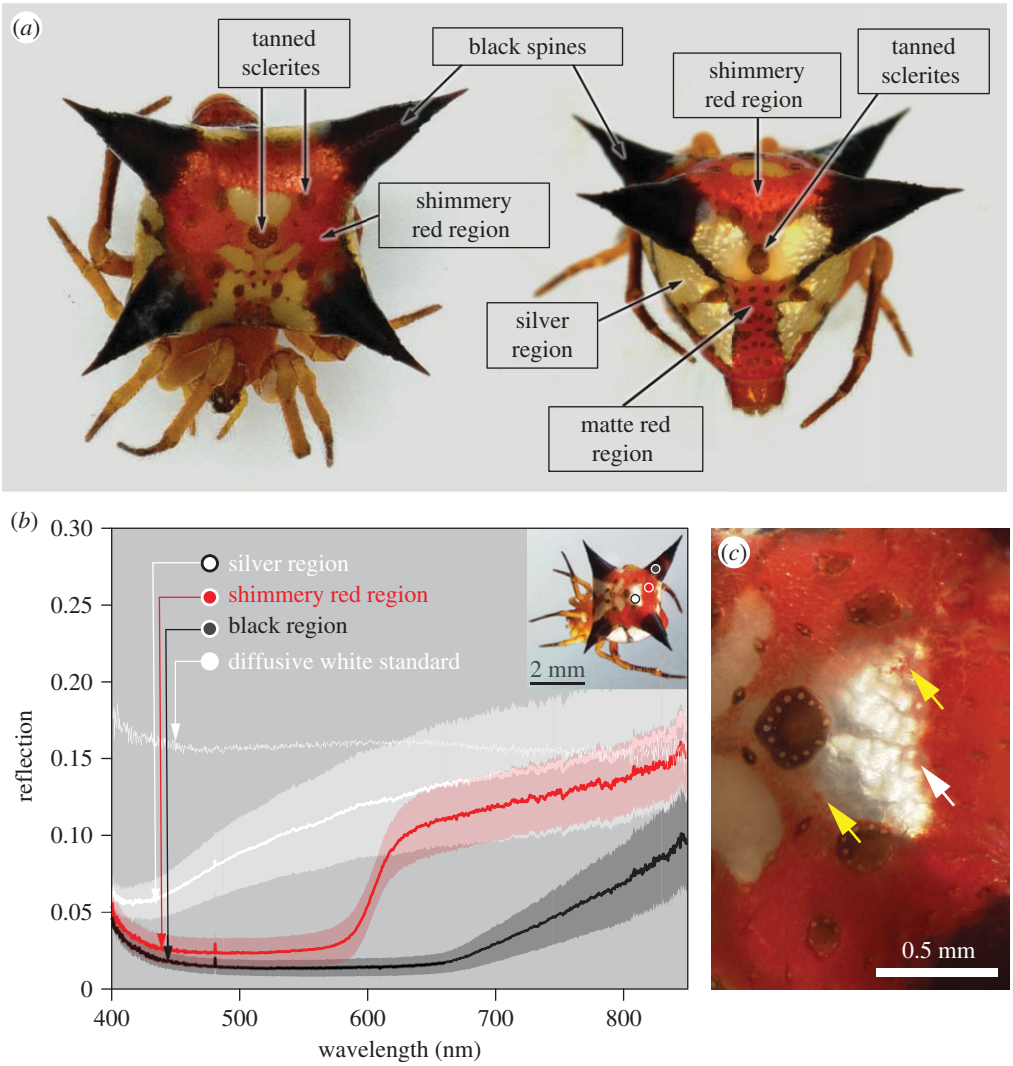

Figure 2. Optical properties of *P. rubroargentea*. (*a*) Dorsal (left) and posterior (right) view of a *P. rubrargentea* specimen with different regions of coloration indicated (CASENT 9057540). (*b*) Reflection spectra taken from three different regions: silver, shimmery red and black regions. The shaded areas represent the spread of original data (greater than 10 measurements for each type) and solid lines are the averaged data. The reflection strength of a diffuse white standard is shown for comparison (MCZ IZ 50966). (Inset) A top-viewed image of *P. rubroargentea*, where the circles indicate the regions of optical measurement (CASENT 9057540). (*c*) A high-magnification optical image showing the silver and red regions. The white arrow indicates the boundary between shimmery red and silver regions. The yellow arrows indicate the locations where isolated red patches are found in the silver region.

Fluorescence is a molecular phenomenon wherein molecules, also known as fluorophores, become excited by absorbing light at a particular frequency (usually higher energy/shorter wavelength) then quickly re-emitting light at a slightly lower frequency. Fluorescence in arachnids is most commonly found in scorpions [35–37], but most spiders have diffusely distributed fluorophores in their haemolymph and many families of spiders have a great intensity of fluorophores in regions of their bodies such as in their cuticle and in setae [38–40]. Fluorescent colours have been detected in many families of spiders ranging in colour from red in *Araneus diadematus* Clerk, 1757 (Araneidae), to dark blue in *Dysdera crocata* C. L. Koch, 1838 (Dysderidae) and a single broad gold-colour peak in *Enoplognatha ovata* Clerck, 1757 (Theridiidae) [38].

With nearly 47 500 described species of spiders in more than 100 recognized families [41], our understanding of the mechanisms and functions of coloration in this diverse group has been limited and remains rich territory for further exploration [9,12,20,22,26,42–45]. Moreover, unlike birds, butterflies and beetles, whose structural colour usually remain and can be observed for centuries (they are typically pinned and kept in dry storage when curated in museum collections), spiders (and other arachnids and fish) are typically preserved using 'wet' preservation methods (70–80% ethanol) to maintain the integrity of the animals' morphology in museum collections. In this case, most of these colours do not withstand long-term storage in collections and usually rapidly degrade (often within a few months). It is thus rare to find vibrantly coloured animals among spider specimens when the animals are curated in this way, and especially rare to find animals that can maintain their colour for years, let alone decades at a time.

In this study, we investigate the striking colorations in the tropical theridiid spider, *Phoroncidia rubroargentea* Berland, 1913, a small, brightly coloured spider from Madagascar (figure 1). Our study was motivated by the observation that specimens of this species usually retain vibrant coloration after storage in ethanol for decades (e.g. MCZ#142197). *Phoroncidia rubroargentea* was first described by Berland in 1913 from two female specimens found in Madagascar in the forest 'Tanala, between Savondron et Andranomafana' [46]. Since that time, they have only been found on the island of Madagascar and can be considered endemic

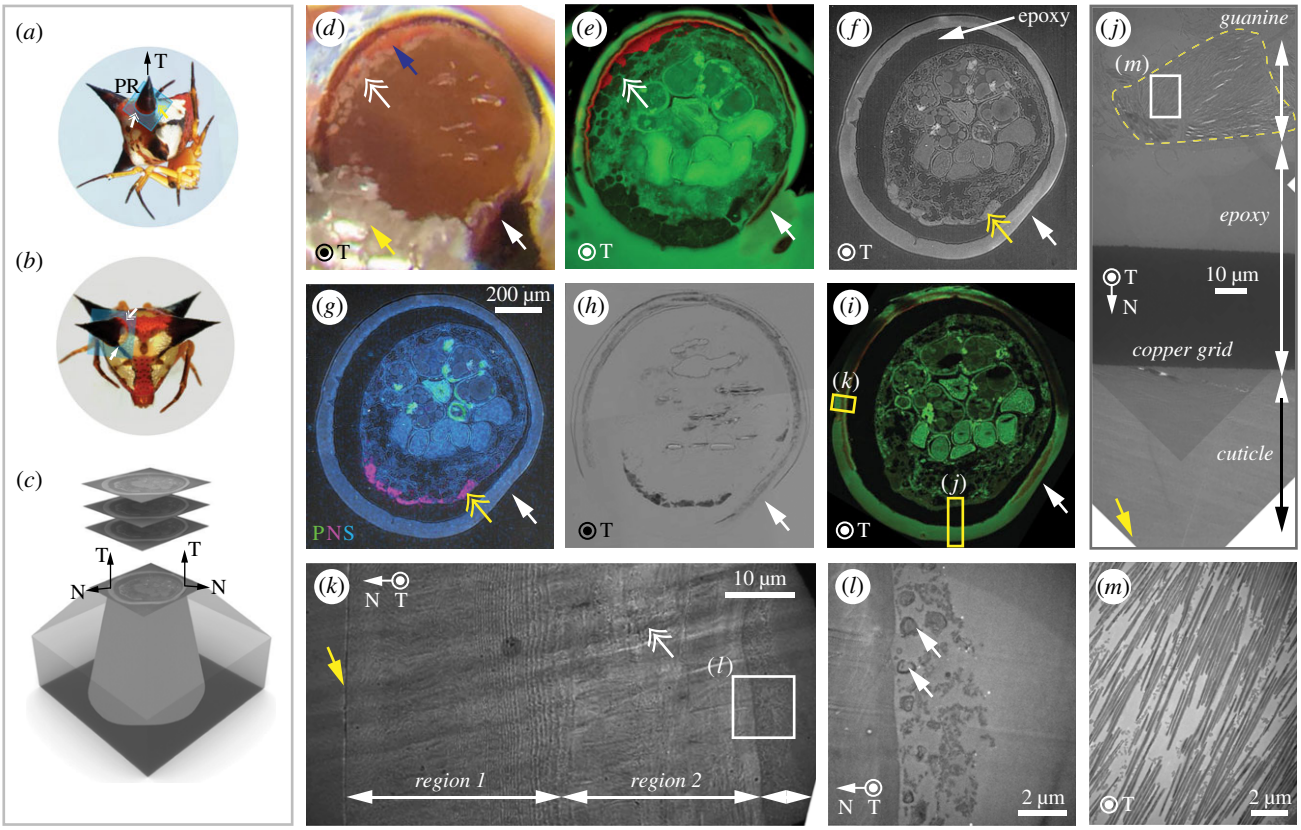

Figure 3. Structural and optical analysis of the spider *P. rubroargentea*. (*a*) Side- and (*b*) front-viewed optical image of the spider specimen (CASENT 9057540). The cross-sectional cut plane (blue section) is shown to indicate that the posterior right (PR) spine was chosen for structural analysis. (*c*) A three-dimensional schematic diagram indicating the orientation of the cross-sectional cut relative to the spine. A cylindrical coordinate system was used, where T and N denote 'tip' of the spine and 'normal' of the cuticle surface respectively. (*d*) Optical image, (*e*) three-dimensional reconstruction from confocal data, (*f*) backscattered electron microscopic (BSEM) image and (*g*) energy dispersive spectroscopy (EDS) map of the cross-sectioned cutting plane of the embedded sample. White single arrow: black region; blue arrow: shimmery red region; yellow arrow: silver region; white double arrow: guanocytes underneath the red region; yellow double arrow: regions with high content of guanine crystals. (*h*) Transmission optical image and (*i*) confocal image of cross-sectional slices. Images in (*d*–*i*) are in the same orientation and magnification, which were acquired from the same region of the embedded sample. Transmission electron microscopy (TEM) images of the cross-sectional slices in the (*j*) silver and (*k*) red regions. Their locations are indicated with yellow boxes in (*i*). The yellow arrows indicate the exterior surfaces of cuticle. The yellow dash line in (*j*) highlights a single guanocyte cell. The white double arrow indicates a region without the cuticular laminated structure. The high-magnification TEM images of the (*l*) red and (*m*) silver regions taken from (*k*) and (*j*), as indicated by the white boxes, respectively. The white arrows in (*l*) indicate the hollow microspheres.

and rare. A few specimens were found during the first two expeditions led by Kariko in the early 1990s, but subsequent attempts to find them during a similar time period in Ranomafana National Park were unsuccessful and there are only a few specimens in museum collections worldwide. For this study, we examined specimens from the Museum of Comparative Zoology's (MCZ) collections, which includes specimens from Kariko's expeditions in the 1990s as well as a 40-year-old specimen collected by W. L. and D. E. Brown in 1977 (MCZ IZ 143122). Specimens from the California Academy of Science (CAS) were also used for this study. Additionally, an attempt was made to examine the more than century-old holotype in Paris to record the colour; however, at this time, the specimen could not be located.

Phoroncidia is a genus in the Theridiid family, the fourth most diverse spider family with 2487 species in 124 genera [41]. The genus has 81 species described to date [41]. *Phoroncidia* occur worldwide, excluding any records to date from northern Europe, Polar regions and western North America. *Phoroncidia*'s phylogenetic relationships remain unresolved—the genus has many morphological characteristics of the Theridiid family but is also considered atypical in many regards due to the lack of a Therdiid-style tarsal comb and abdominal stridulating organ [47–49]. Seven species of *Phoroncidia* have been described from Madagascar: *Phoroncidia ambatolahy* Kariko, 2014, *Phoroncidia aurata* O. Pickard-Cambridge, 1877, *Phoroncidia quadrispinella* Strand, 1907, *Phoroncidia roseleviorum* Kariko, 2014, *Phoroncidia rubroargentea* Berland, 1913 *Phoroncidia vatoharanana* Kariko, 2014 and *Phoroncidia wrightae*, Kariko, 2014 [50]. As a group, the species of *Phoroncidia* from Madagascar are colourful and often metallic, for example *P. wrightae* appears almost leopard spotted—with golden coloured sclerites rimmed in black on a silver background; females of *P. ambatolahy* are often a vibrant green; females of a yet undescribed species of *Phoroncidia* are similarly red, silver with four black spines; and females of *P. vatoharanana*'s abdomens are silver flecked and black [50] (electronic supplementary material, figure S1).

In this study, we aimed to understand structural and compositional origins of the vibrant colours displayed in the spider *Phoroncidia rubroargentea* and to understand what factors contribute to their apparently unique ability to maintain vibrant colour in long-term storage in ethanol. We use multi-scale correlative structural, chemical and optical characterization techniques to elucidate the structural origin of its combination of coloration patterns based on red,

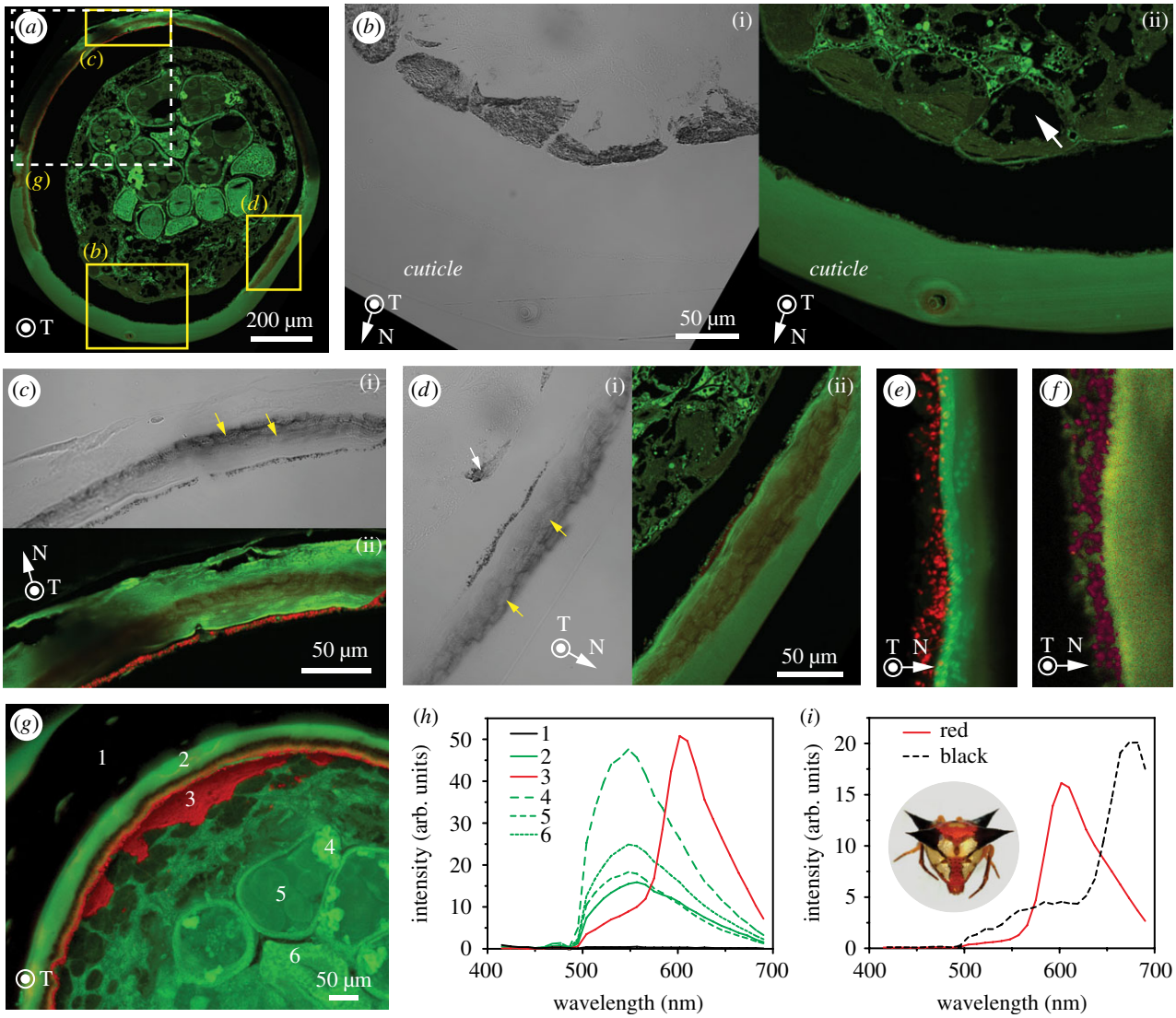

Figure 4. Optical analysis of structures with different colours (CASENT 9057540). (*a*) Confocal fluorescent image of a thin slice for the intact cross section of the spine region. (*b–d*) Transmission optical (i) and corresponding confocal fluorescent (ii) images for three different regions acquired from (*b*) silver, (*c*) red and (*d*) black regions, respectively. The white arrow in *b* (ii) indicates the region within a guanocyte deprived of guanine crystals. Their locations are indicated in (*a*). The yellow arrows in *c*(i) and *d*(i) indicate the pigmented portion in the cuticle. The white arrow in *d*(i) indicates the presence of guanine crystals. Three-dimensional reconstruction based on confocal measurement for (*e*) red and (*f*) black region. (*g*) A three-dimensional rendering of the microtomed block in the red region based on confocal measurement. (*h*) Fluorescent spectra taken from different regions (indicated by numbers) shown in (*g*). Note the distinct red fluorescence in the red coloured region. (*i*) Fluorescent spectra acquired for red and black regions in (*e*) and (*f*), respectively.

silver and black colours. Our findings suggest that a combination of fluorescent pigmentation based on microscopic spherical structures and broadband reflection based on guanine platelet-like microcrystals create the vibrant colour and patterns found in *P. rubroargentea*.

2. Material and methods

2.1. Specimens

The following specimens were examined for this study from collections at the Museum of Comparative Zoology (MCZ) and the California Academy of Sciences (CAS): (MCZ IZ 143122, 32022, 50966, 53933, 54189); (CASENT 9057540, 9003201, 9057570, 9057533, 9057528, 9057542, 9057554, 9057519, 9057544, 9002297, 9002378, 9002420, 9003465). Prior to experiments, the specimens were stored in 70–80% ethanol. Experiments were conducted on these specimens in the following ways: (MCZ IZ specimen 50966): used for optical measurements (figure 2), scanning electron microscopic (SEM) imaging of the fractured abdomen through a silvery region (figure 5*c*,*d*; figure 7*a–d*); (MCZ IZ 143122): observed in the field before storing in ethanol and performing optical measurements (figure 1*e*,*f*); (CASENT 9057540): SEM, energy dispersive spectroscopy (EDS), confocal microscopy, optical imaging (figures 2*a*,*b*, 3, 4, 5*e–h*, 6 and 7*e*,*f*); (CASENT 9057540C): removed Leg IV (electronic supplementary material, figure S8). Experimental remains of these specimens will be stored at the respective institutions: for MCZ IZ specimens at the Museum of Comparative Zoology and for CASENT specimens at the California Academy of Sciences. Images of MCZ specimens are credited to the Museum of Comparative Zoology, Harvard University © President and Fellows of Harvard College.

2.2. Optical measurement

Specimens were examined after being cleaned by gentle agitation in vials of ethanol (70%) and by removing debris using soft-tipped brushes. Spiders were positioned for imaging using featherweight forceps and watercolour paintbrushes, and examined using a Leica 12\5 microscope with Leica Planar 1.0 and 1.6× objective

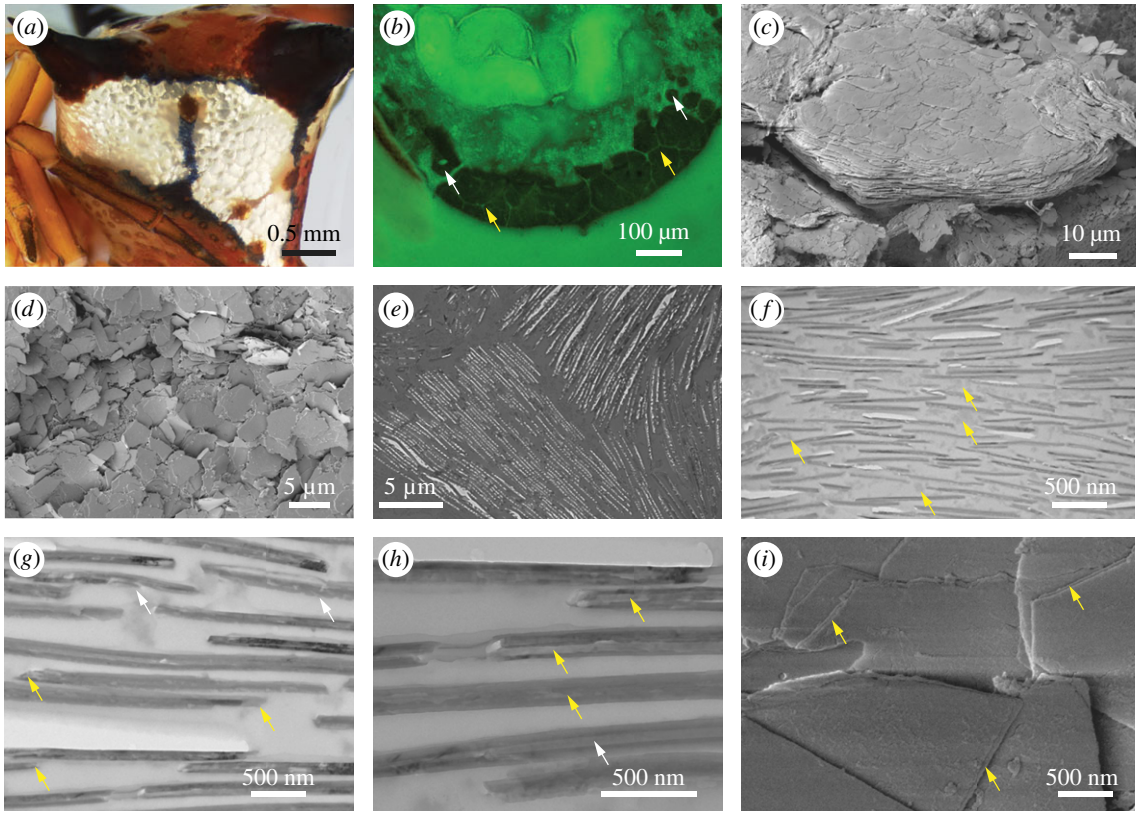

Figure 5. Structural characteristics of the guanine microplates in the silver regions. (*a*) Optical image of the silver region, where individual guanocytes are visible. (*b*) A three-dimensional rendering of the microtomed block in the silver region based on confocal data. Note the low intensity in the silver region due to strong directional reflection. The yellow arrows indicate the grain boundary junctions among adjacent guanocytes. The white arrows indicate the immature circular-shaped guanocytes. (*c*) A scanning electron microscopy (SEM) image of an individual guanocyte, showing multiple layers of guanine crystals (MCZ IZ 50966). (*d*) An SEM image of guanine crystals (MCZ IZ 50966). (*e–h*) Bright-field TEM images of guanine crystals (CASENT 9057540). Note that usually even within the same guanocytes, the guanine crystals may exhibit different orientations (*e*). The yellow arrows in (*f*) indicate the presence of globular substance within the spacing of guanine microplates. The white and yellow\arrows in (*g*) indicate the rough surface and irregular edges. The doublet structures in the individual guanine crystals can be clearly seen in (*h*). The yellow and white arrows in (*h*) indicate the rough and smooth interfaces between the outer crystals and inner region. (*i*) High-magnification SEM image showing the doublet structures (yellow arrows).

lenses. Images were taken in lateral, dorsal and ventral views employing focus-stacked light micrographs, using a Leica MZ 12\5 microscope with a Leica 1.6 objective lens connected by Leica 0.63× mount connector, attached to a JVC 3CCD digital camera. Images were processed in Adobe Photoshop and organized using Adobe Illustrator CS4. Photos and measurements were made with Auto-Montage software and are in millimetres unless noted otherwise. Optical spectra were acquired from the different coloured regions of the specimen with micro-scale resolution using a modified optical microscope (Leica DMRX). Samples were illuminated in the area of interest with a halogen lamp in reflection mode. A 50/50 beam-splitter in an additional microscope port allowed for confocal collection of light from specimen target areas between 1 and 50 µm diameter, depending on the employed objective (50× to 10× magnification). This light was captured into a 50 µm core optical fibre connected to a grating spectrometer (Maya 2000 Pro, Ocean Optics). All spectra are referenced against a flat silver mirror of ≥95% reflectance in the wavelength range of 400–800 nm.

2.3. Electron microscopy

Samples were coated with ultra-thin carbon or Au to reduce charging effects prior to SEM imaging with a Helios Nanolab 660 Dual Beam electron microscope (FEI, OR) at an acceleration voltage of 5 kV and a working distance of approximately 4 mm. Low magnification SEM images shown in figure 4 were acquired with a Tescan Vega GMU SEM with acceleration voltage of 20 keV. Energy dispersive spectroscopy (EDS) measurements were acquired from the same system equipped with a Bruker X-Flash EDS system at an acceleration voltage of 20 kV.

TEM samples were prepared using a standard embedding and microtoming technique. Typically, the samples (in 70% ethanol) were rehydrated sequentially with in a stepwise fashion from the original 70%, to 50% (30 min), to 30% (40 min) and water (20 min). Each specimen was then punctured above the base of the pedicel and between the two anterior spines by inserting a blade tip before fixation in a solution of 4% paraformaldehyde, 1% glutaraldehyde and 0.1 M HEPES overnight. The fixed sample was then washed with 0.1 M HEPES (10 min), three times and then by milliQ water (15 min) on ice four times. The washed sample was then dehydrated sequentially with increasing concentration of ethanol at low temperatures: 50% ethanol on ice (45 min); 70% ethanol at −20°C (30 min) and 95% ethanol at −20°C (30 min). The sample was infiltrated with ethanol/London Resin (LR) white mixture with increasing resin concentrations: 1 : 1 ethanol : LR white at −20°C for overnight; 7 : 3 ethanol : LR white at −20°C for 1 h; LR white at −20°C for 1 h. The final polymerization step was performed in an oven (DX300 Yamato Gravity convection) at 50°C overnight after the specimen was put in LR white in an oven-dried gel capsule with its spines pointing down. After the resin was polymerized, the gel capsule was first removed, and the bottom of the resin block was trimmed with a razor blade. The specimen was sectioned (Leica Ultracut UCT, ultramicrotome) with both diamond and glass knives (the glass knives were made using a glass knife maker (Leica E, KMR2)). Typical

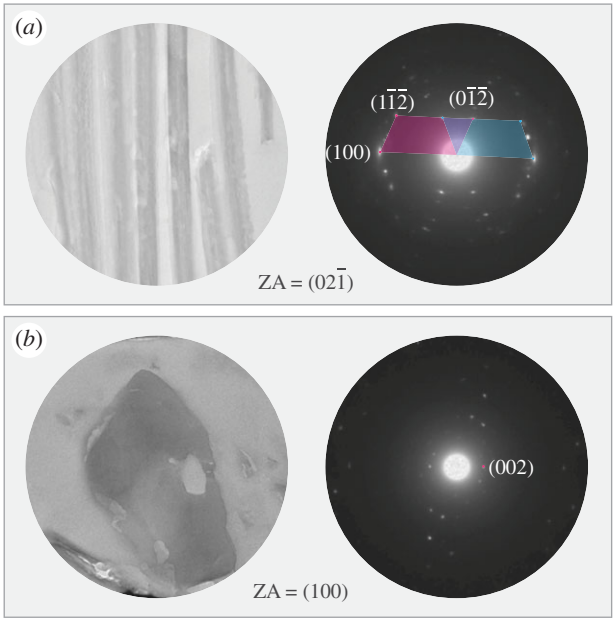

Figure 6. Crystallographic characteristics of the guanine microplates (CASENT 9057540). Bright-field TEM image (left) and corresponding selected area electron diffraction (SAED) patterns for the guanine crystals in two directions: (*a*) edge-on and (*b*) in-plane orientation, respectively. The diffraction patterns were indexed as β-phase anhydrous guanine and have zone axes (ZA) of [02$\bar{1}$] and [100]. The original diffractions are white spots, and the simulation of the electron diffractions are indicated by spots with other colours. For the edge-on orientation, two sets of diffractions were identified, which have a mirror symmetry along the longitudinal direction of guanine microplates.

slice thickness was 50 to 80 nm for TEM imaging and 1 µm for optical and fluorescence imaging. TEM imaging with standard bright-field and SAED techniques was carried out using a JEOL 2011 operated at 120 kV. SAED measurements were conducted on guanine crystals in two orientations, i.e. edge-on and in-plane orientations.

2.4. Confocal measurement

A thin cross-sectioned sample (mounted on a glass slide) was imaged with Zeiss LSM880 super-resolution confocal microscope. Full cross-sectional fluorescence images were obtained with a 10×/0.45 objective using 488 nm excitation and Airyscan detector. Green fluorescence was collected with 495–550 nm band-pass filter and red fluorescence with 605 nm long-pass filter. Transmitted light images were obtained with 40×/1.3 oil immersion objective and 488 nm illumination using transmitted light PMT detector. Z-stacks of the microtomed block were acquired with the LSM880 with 10×/0.45 objective and 488 nm excitation using a 32 channel spectral detector. Green and red fluorescence signals were separated with linear unmixing after acquisition. Images and 3D movies of the stack were rendered with Imaris 8. Fluorescence spectra corresponding to different regions in the samples were obtained by acquiring spectral images (as above) and by averaging the pixel-level spectra over the corresponding regions indicated in the main text. Excitation intensity and detector gain were kept constant for all spectra in figure 4*h*. Excitation intensity was kept constant for the spectra in figure 4*i*, but higher detector gain was used for the 'black' signal due to its weaker intensity compared to the 'red'.

2.5. Fluorescence imaging

Intact spider samples in 70% ethanol were imaged using a Zeiss Axio Zoom V16 fluorescence microscope equipped with PlanNeoFluar Z 2.3×/0.57 objective, HXP 200C metal halide illuminator and Hamamatsu Flash 4.0 v2 sCMOS camera. Apotome 2 was used to obtain optical sections. Green and red fluorescence channels were acquired separately using GFP (Ex. 450–490 nm, Em. 500–550 nm) and RFP (Ex. 559–585 nm, Em. 600–690 nm) filter sets, respectively, and merged with Zeiss Zen Blue software. 3D movies were rendered with Imaris 8.

3. Results

Specimens of *P. rubroargentea* used in this study were collected primarily in central domain rainforests in Madagascar (figure 1*a*,*b*). *P. rubroargentea* are small animals approximately 3 mm long, and live animals reveal bright silvery reflections on the side of the body and red coloration at the base of black spines (figure 1*g* and figure 2*a*). Members of the genus are recognized by a distinctive genital morphology and a sclerotized ring surrounding the spinnerets, with a colulus often replaced by two setae [51]. As shown in a series of optical images of a *P. rubroargentea* specimen viewed at different orientations (figure 1*g*), the abdomen of *P. rubroargentea* resembles a cube with the four corners extended into sharp cones or spines. The four sides of the abdomen are primarily covered with highly reflective silvery patches. On the dorsal surface of the abdomen, the four spines appear black. In addition to silvery and black regions, two types of red coloration are distributed on the spider's body surface. A strip of matte red extends from the base of the spinnerets midway up the posterior side of the abdomen with silvery regions on either side (figure 1*g* and figure 2*a*). Portions of the bases of the spines appear matte red as well. In addition, the majority of the dorsal surfaces have a shimmery red appearance. As discussed later, the shimmery red regions are where red particles co-localize with guanine plates, and matte red is where no guanine plates are present beneath (figure 2*a*; electronic supplementary material, figure S8). As noted earlier, the silver/red coloration pattern usually remains unchanged after the specimens have been stored in 70–80% ethanol for long periods, and a museum sample collected in 1977 still retains vibrant colour 40 years later (figure 1*d*). This is in stark contrast to virtually all other spider specimens preserved in ethanol. For example, after storing in ethanol for 220 days, the colour was degraded dramatically for the spider *Theridula emertoni* Levi, 1954 a species in the same family as *Phoroncidia* and of a similar size (figure 1*e*,*f*).

Reflection spectra from the different coloured regions on the spider's body were acquired using microspectrometry. The silvery regions exhibit a high reflectance over the whole visible range, comparable to a diffuse white reflection standard (figure 2*b*). The reflection spectra taken in the shimmery red regions exhibit very low reflection intensity (approx. 2%) in the blue-green spectral region and increase sharply at a wavelength of approximately 600 nm. In comparison, the spectra acquired from the black spines have very low reflectivity for nearly the entire visible range, despite a slight increase in the red and near-infrared wavelength (greater than 700 nm). The matte red regions show decreased reflection intensity in the red wavelength by approximately 20% compared to the shimmery red regions (electronic supplementary material, figure S2). Additional details from the microspectrometric analysis are summarized in electronic supplementary material, figure S2. Figure 2*b* inset shows a dorsal view of a *P. rubroargentea* specimen

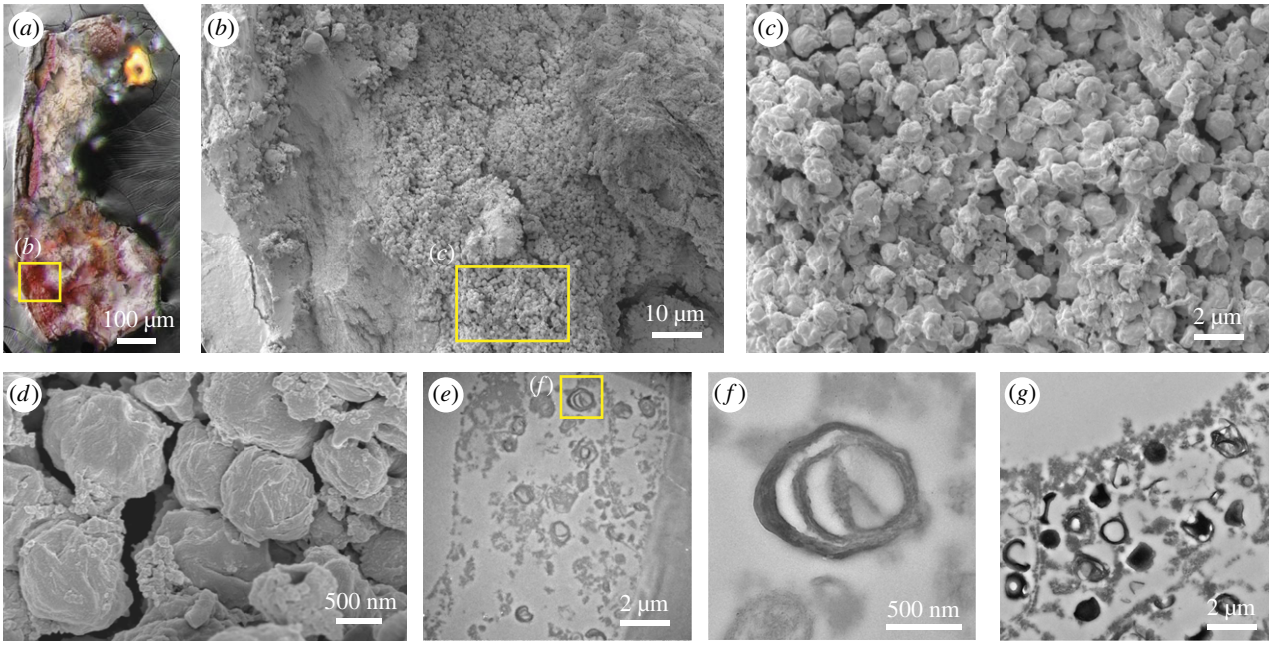

Figure 7. Structural analysis of the red regions. (*a*) An overlaid image based on SEM and corresponding optical image of a fractured piece of the spider's abdomen. This allows direct identification of structural features corresponding to the red colour (MCZ IZ 50966). (*b–d*) A series of SEM images at different magnifications taken from the red regions. Note that characteristic microspheres with rough surfaces were observed (MCZ IZ 50966). (*e*) Cross-sectional TEM image of the red region, where hollow spherical structures were identified (CASENT 9057540). (*f*) TEM image of an individual microsphere (adapted from *e*), showing its hollow internal structure (CASENT 9057540). (*g*) TEM image of another type of microspheres with dense internal structure acquired from the black region.

and locations of measurement shown in figure 2*a* are indicated. A high-magnification optical image of the top central area of the spider abdomen reveals that there appears to be a gradual transition from the shimmery red to the silver regions (figure 2*c*, white arrow). In addition, isolated red patches distributed in the silver region are observed (figure 2*c*, yellow arrow), which suggests that the silver region may be located directly beneath the red region.

To determine the constituent materials and structures at the origin of the spider's varied colour display, we conducted correlative structural analysis by using bright-field and fluorescent microscopy, electron microscopy and energy dispersive spectroscopy (figure 3). An intact specimen was embedded in resin after the posterior right (PR) spine was positioned towards the cutting plane (electronic supplementary material, figure S3). Microtoming was then used to produce thin slices along the cross sections of the PR spine (figure 3*a*,*b*). A pseudo-cylindrical coordinate system was used for denoting the sample orientations, where T refers to the tip of the spine and N and C refer to the surface normal and circumferential directions, respectively (figure 3*c*).

Figure 3*d* depicts the cutting plane of the embedded block, which captures the silver region (yellow arrow), the red region (blue arrow) and the black region (white single arrow) in the same slice. Moreover, silvery plates are observed underneath the red patches (white double arrow). The same embedded block was examined with confocal microscopy. Owing to the transparent nature of the embedding resin, we were able to collect *z*-stack confocal microscopic images, which allowed us to reconstruct the structure in 3D (figure 3*e*). It was found that the red region exhibits a pronounced red autofluorescence (excitation wavelength = 488 nm), while the majority of the remaining structure displays green autofluorescence (figure 3*e*). The white double arrow indicates the location of guanocytes underneath the red region, consistent with observations shown in figure 3*d*. They appear black in this image due to the fact that the guanine platelet-based mirrors reflect the excitation light and, therefore, do not allow for fluorescent excitation of the underlying material. Electronic supplementary material, movie S1 shows a 3D reconstruction from the confocal microscopy data, which clearly reveals the relative location of red and silver regions. Moreover, regions corresponding to the black spines on the spider's abdomen display a cuticle that appears to differ from the multi-layered cuticle structure in the red and silver regions. The cuticle in the black areas has a slightly tanned or pigmented appearance with patch-like structures of approximately 10–15 µm in size and is discussed in more detail later. The microtomed block surface was examined using backscattered electron microscopy (BSEM, figure 3*f*) and energy dispersive spectroscopy for compositional analysis (figure 3*g*). The BSEM image revealed that the outer cuticle layer has a relatively constant thickness (60–80 µm, figure 3*f*), with contrast varying as a function of electron density. EDS mapping through the silvery guanine region reveals a high nitrogen content, as expected from the chemical composition of guanine (electronic supplementary material, figure S4). Moreover, careful examination reveals some subtle variation in elemental distribution within the cuticle layer. More specifically, the cuticle region directly on top of the slivery region exhibits a very uniform chemical composition, whereas the cuticular regions above the red and black regions exhibit a minute but detectable increase in sulfur content (figure 3*g*, electronic supplementary material, figure S4). This compositional variation within the cuticle layer seems to be closely correlated with the variations observed in the bright-field transmission and fluorescence images (figure 3*h*,*i*). Detailed descriptions of the two imaging results are summarized in figure 4 and will be discussed later.

The gap between the central structural region and the outer cuticular layer represents an artefact caused by the embedding resin, which may have resulted from the shrinkage of soft internal structures upon storage in ethanol. This claim is supported by a number of observations. First, the top profile of inner structures and the bottom profile of the cuticle layer resemble each other and exhibit similar curvature (figure 3*h*). Moreover, the gap region shows a similar grey value as in the resin in BSEM image (figure 3*h*) and like the exterior resin areas does not show fluorescence (figure 3*f*).

Ultra-thin slices (thickness, approximately 80 nm) were also collected at similar locations on the embedded sample for transmission electron microscopic (TEM) analysis (figure 3*j–m*). Figure 3*j* shows an overview TEM image taken from the guanine region as indicated in figure 3*i*. The cuticle in this region exhibits a characteristic chitin-based multilayer structure as observed in typical cuticle structures in other arthropods [10]. In addition, the thickness of individual chitin layers gradually increases towards the inner region (see electronic supplementary material, figure S5). Beneath the cuticle layer, guanocyte cells containing guanine microplates are observed (indicated by the yellow contour in figure 3*j*). In general, the longitudinal direction of guanine microplates is parallel to the exterior surface of the cuticle, despite some localized orientational variations (figure 3*j*). Figure 3*m* shows a high-magnification view of guanine microplates, where individual guanine microplates are visible.

Figure 3*k* shows a TEM image taken from the red region (as indicated in figure 3*i*). Compared to the cuticular structure in the guanine region, a similar chitin multi-layered structure is observed in the outer region of the cuticle (region 1, approximately 30 µm); however, such layered structure is absent at the inner region of the cuticle (region 2, approximately 30 µm). Patches with size of 10–20 µm with heterogeneous contrast were observed (white double arrow), consistent with optical observations (figure 4). Moreover, spherical and other irregular shaped microstructures (approx. 1 µm, white arrows in figure 3*l*) were present beneath the cuticle, spanning a region of 2–5 µm in the vertical direction (figure 3*l*). As discussed later, these microstructures are responsible for the red coloration.

Additional correlative optical transmission and fluorescence imaging on different structural types based on the same cross-sectional slices are summarized in figure 4. The cuticle layer associated with the guanine region exhibits uniform transmittance and green fluorescence (figure 4*b*) and the boundaries of individual guanocyte cells can be observed clearly in the fluorescence image. Guanine microplates are typically located in guanocytes towards the exterior direction, while the inner portion is absent of structural features, as indicated by high transmittance and low fluorescence in the two images. In comparison to the uniform optical appearance for the cuticle located directly above the guanocytes, the cuticular layer associated with the red and black regions exhibits two sublayers with distinct optical features (figure 4*c*,*d*). The exterior portion of the cuticle exhibits similar high transmission and fluorescence to other cuticle regions, whereas the inner portion appears dark and red/brown in colour in the transmission and fluorescent images respectively. Additionally, the coloration within these regions is not uniform, where patches with slightly less pigmentation were observed and the boundaries typically are darker and more red/brown (yellow arrows in figure 4*c*(i) and *d*(i)), and are thus likely to be the same structure observed in TEM images (figure 3*k*). In addition, directly beneath the cuticle layer, particles with strong absorption and red fluorescence in the red regions were identified. 3D reconstruction of individual microparticles in figure 4*e* indicates that the particles show nonspherical fluorescence distributions. On the other hand, the microparticles observed in the black region appear to be more solid microspheres (figure 4*f*). The white arrow in figure 4*d* also indicates the presence of guanine crystals directly beneath the red region (also see electronic supplementary material, figure S6).

Fluorescent emission spectra were taken from multiple regions of the microtomed block (figure 4*g*,*h*). The majority of the tissue exhibit green fluorescence with a peak position of approximately 550 nm. The red region, despite the presence of a secondary shoulder in the green range, has a peak position at 610 nm. In comparison to the red region, the black region exhibits a fluorescence peak at 680 nm (figure 4*i*).

The guanocytes and their guanine microplates were characterized at multiple length scales by using a combination of microscopic techniques (figures 5 and 6). Direct observation of the spider body reveals that the silvery region consists of patches with pseudo-hexagonal geometries (approx. 100 µm in diameter), corresponding to individual guanocytes (figure 5*a*). The boundaries between adjacent guanocytes can be more clearly seen from SEM images acquired from interior surface from the fractured regions through the abdomen (electronic supplementary material, figure S7). This can also be visualized through the 3D reconstruction from the confocal microscopy data (figure 5*b*). Individual guanocyte cells appear as dark patches due to strong reflection in other directions, and thin boundaries with high green fluorescence are observed among adjacent cells. We noticed that the contact angles at the triple junctions of adjacent guanocytes are close to 120° (yellow arrow, figure 5*b*). Moreover, at the edge of the guanocyte region, small, isolated circular guanocytes were observed (white arrow, figure 5*b*), which may be guanocytes in the formation process. Figure 5*c* shows a guanocyte packed with guanine crystals after the exoskeleton was fractured. Figure 5*d* shows a representative morphology of guanine microplates, which usually do not generally exhibit any faceted morphologies. Figure 5*e* shows a TEM image of the guanine crystal assembly located within one guanocyte cell, which consists of multiple domains with co-aligned guanine microplates. The size of the guanine microplates was measured to be 3.6 ± 1.7 µm ($n = 118$). In addition, short crystals without long-range order are observed towards the interior of the body, which corresponds to isolated guanine crystals observed in optical imaging (figure 4*b*). Structures with darker contrast compared to embedding resin with irregular geometries were observed in between the crystals (yellow arrow, figure 5*f*,*g*).

High-magnification TEM imaging allows us to examine the fine structural features for individual microplates (figure 5*g*,*h*). From these studies, it was revealed that the crystals exhibit many structural defects, such as surface roughness (white arrows) and irregular edges (yellow arrows, figure 5*g*). Moreover, each individual guanine crystal appears to be in a doublet structure consisting of two outer

layers separated by an observable space with less electron density (arrows in figure 5*h*). The two outer layers have roughly similar thickness of 30–40 nm and the total thickness of each guanine microplate is 110.7 ± 22.8 nm ($n = 134$). The boundaries between the central and two outer layers exhibit two types of morphologies, i.e. rough and smooth interfaces, respectively (yellow and white arrows, respectively in figure 5*h*). The doublet structure can be also observed at the edges of individual guanine microplates from oblique angles in SEM images (arrows in figure 5*i*).

We next studied the crystallographic characteristics of the guanine crystals by selected area electron diffraction at two orientations, i.e. plan view and cross-section (figure 6). It is known that guanine crystallizes in a monohydrate phase ($P_{21/n}$, $a = 16.51$, $b = 11.27$, $c = 3.645$ Å, $\beta = 95.88$) [52] and two polymorphs of the anhydrous phase, i.e. α and β ($P_{21/c}$, $a = 3.56$, $b = 3.59$, $c = 6.38$ Å, $\beta = 118.5$ [53], and $P_{21/n}$, $a = 3.59$, $b = 9.72$, $c = 18.34$ Å, $\beta = 119.5$ [54]). Only anhydrous β-phase guanine has been reported to be present in biological systems. All the electron diffraction peaks for the vertical orientation can be accounted for by assuming either the α or β polymorph. There are three sets of strong reflections in one configuration (red spots), which include the (100) ($d_{100} = 3.13$ Å), (012) ($d_{012} = 6.21$ Å), and ($1\bar{1}\bar{2}$) reflections ($d_{1\bar{1}\bar{2}}$=3.31 Å) (figure 6*a*). The corresponding zone axis for this diffraction pattern is 2*b*-*c*, in other words [02$\bar{1}$]. Most importantly, an additional equivalent set of diffraction data (blue spots), related to the red set by mirror symmetry is observed, which we interpret in terms of a twinned structure about the [02$\bar{1}$] axis. This twinned structure may be related to the observed doublet structure in the guanine crystals. The diffraction pattern in the horizontal direction exhibits an unambiguous (00*l*), $l = 2n$, diffraction line which excludes the α form and is indicative of the β form (figure 6*b*). However, the diffraction pattern also appears to exhibit a set of (0*kl*) diffraction peaks as if arising from stacking faults composed of at least two layers as suggested in the case of biogenic fish crystals [54]. We, therefore, conclude that the guanine crystals found in this spider species are doublets of the β anhydrous form, twinned about the [02$\bar{1}$] axis.

The detailed structural analysis at multiple length scales for the red region is summarized in figure 7. The red region of the spider cuticle was fractured for sequential optical and electron microscopic analysis. Correlating optical and electron microscopy images of the specimen allowed us to determine the structural types responsible for the red coloration, as shown in an overlaid optical and SEM image (figure 7*a*). Spherical structures with a typical diameter of approximately 1 µm are observed in the red region (figure 7*b–d*). The surface of the microspheres appears to be corrugated and rough; a layered morphology can be observed in high-magnification SEM images. In addition, some microspheres have holes or indents, which leads to non-spherical features, consistent with the confocal tomography data (figure 4*e*). Figure 7*e* shows a TEM cross-sectional image taken from the red region, which reveals the internal structure of the microspheres from the microtoming cut. The microspheres usually exhibit a spherical shell-like architecture with multiple layers within each microsphere (figure 7*f*). Moreover, TEM images taken from the black region reveal another microsphere structure with dense internal morphology, in stark contrast to the internally layered microspheres (figure 7*g*). This structural difference between the two types of microsphere structures found in the red and black regions may explain the observed difference in fluorescence distributions within individual particles (figure 4*e,f*).

For some specimens, we found that the red coloration sometimes depends on the intactness of the outer cuticle layer. As shown in electronic supplementary material, figure S8, the red coloration disappeared after one of the legs was removed and the specimen was stored in ethanol for about a month (electronic supplementary material, figure S8D–F). However, the silvery appearance was retained during this process. This also directly shows that the shimmery red region is usually associated with the presence of guanine crystals underneath (electronic supplementary material, figure S8B, E), whereas the matte red regions are deprived of guanine crystals (electronic supplementary material, figure S8A, D).

4. Discussion

In this work, we present a detailed characterization of the multiple structures and their relationships that produce colour in the spider *P. rubroargentea* by correlating structural, elemental, optical and fluorescent measurements. We find that microscopic guanine platelets are responsible for the overall silver appearance, whereas microspheres with complex internal structures are strongly absorptive and fluorescent, producing the red coloration. The red microspheres are also often located on top of guanine crystals, and this combination is believed to increase the visibility of the red reflection. We also observed that the thick cuticular layers are modified locally to interact with the underlying optical elements to produce the complex coloration patterns.

Unlike inorganic biominerals, only a small number of organic crystals have been found in biological systems, among which crystalline guanine is one of the most widespread. In the animal kingdom, guanine crystals have been mainly found in three phyla: Chordata, Arthropoda and Mollusca. Among these organisms, guanine in crystalline form is usually used for optical purposes, and the metallic and silvery iridescence of fish skin is perhaps one of the most common and striking examples. As summarized in a recent review article by Gur *et al*. [55], typical functional optical performance provided by guanine crystals include light scattering, multilayer reflection (broadband reflection, narrowband reflection, tunable reflection), 3D photonic crystals and mirrored eyes.

Spiders have long been known to produce highly reflective silvery and matt-white effects by using platelet- and cuboid-shaped guanine crystals, respectively [10,20–22]. Millot [20] conducted pioneering work on the nature and distribution of guanine in spiders in 1926, and he pointed out that ‘guanine is stored primarily (or exclusively) as a colorant and not for other, metabolic reasons’. Phylogenetic distribution of the two major types of guanine, matte and silver, show that silver guanine appears to have evolved from matte multiple times, and that matte guanine appears to be the ancestral type; Silver guanine has apparently evolved at least eight times in spiders [21], and guanine is distributed very unevenly across the 113 families of spiders [20,21].

In this work, we identified that the spider *P. rubroargentea* also possesses a multilayer reflection system based on

guanine microplates. The guanine crystals are always located on the exterior-most region of individual guanocyte cells, close to the body surface. TEM observation suggests that guanocytes have very thin membranes where guanine crystals are enclosed. The soft membranes are believed to facilitate the close packing of individual guanocytes beneath the transparent cuticle layer. As shown by direct optical observation and confocal tomography reconstruction, the developing guanocytes, located at the edges of the silvery regions, gradually increase in size until they make contact with adjacent guanocytes. Owing to the soft nature of the guanocyte membrane, the contact lines of adjacent guanocytes exhibit the classical triple-grain junctions, leading to complete areal coverage. Moreover, the correlative observations in the cross-sectional orientations also provide insights into the possible formation process of guanine crystals within guanocytes: they may be formed at the inner side of individual guanocytes and subsequently transported to the outer side, where the alignment of crystals may also take place simultaneously. Further investigation is ongoing to elucidate additional details of this synthesis pathway.

Similar to observations in *Tetragnatha montana* Simon, 1874, another silver-coloured spider, guanine crystals in *P. rubroargentea* do not exhibit defined crystal facets, unlike those in Koi fish, although straight edges are occasionally observed in some guanine crystals (electronic supplementary material, figure S9). In addition, a doublet-structure described previously in *T. montana* is also observed in the guanine crystals of *P. rubroargentea* [22]. Cross-sectional TEM images clearly reveal one inner and two outer layers within individual guanine microplates. The thickness of these three sublayers are roughly similar (30–40 nm), leading to total thickness of approximately 110 nm. The thickness measurement based on microtome cross sections may overestimate the true thickness due to the possible non-orthogonal cutting; however, thickness measurement based on focused ion beam cross-sectional milling, where the cutting orientation was finely controlled, reveals similar results. In the previous study on another spider species, Levy-Lior *et al.* [22] suggested that the material located in the inner region between two crystalline sublayers is not cytoplasm, but amorphous guanine. Our work did not provide direct identification of the materials in the guanine inner layer; however, the structural and crystallographic study in the cross-sectional orientation of guanine microplates provides additional new insights. First of all, the morphology of the inner-outer boundaries varies considerably in individual guanine microplates, where both smooth/straight and rough/wavy boundaries are observed. Moreover, hole-like defects in the crystalline outer layers located in the interior areas of microplates are often observed, which has not been reported earlier (electronic supplementary material, figure S9, white arrows). More importantly, we were able to conduct electron diffraction measurement along the vertical direction, which directly led to the observation of twinning structure about the axis of $[02\bar{1}]$ in individual guanine microplates.

Twinning in biological guanine crystals has been recently reported in copepod and scallops [54]. The twinning structure is shown to allow for high-symmetry morphologies such as hexagonal and square crystals, whereas the guanine crystals in the *P. rubroargentea* spider usually do not show high-symmetry morphologies. To our knowledge, our findings are the first reported observation of twinning in guanine crystals in arachnids, because the twinning structure was not observed in a previous study of guanine microplates in the spider of *T. montana* [22]. This is based on the observation of random superimposed diffraction patterns in the in-plane orientation, although a similar doublet structure was observed [22]. This discrepancy may result from structural differences between different species, as we already observed a great difference in microplate thickness.

The presence of rough sublayer interfaces, defect-like holes and twinning boundaries may provide important insights in understanding the guanine formation mechanisms. Unlike the previous hypothesis of independent nucleation for two crystalline outer sublayers [22], the twinning morphology may have resulted from the formation of one sublayer first, and then acts as a substrate for the second sublayer to form according to the twinning orientation. This may explain the observations of hole-like defects in some crystals where the complete coverage by the overgrown sublayer is not achieved yet. Additional investigation is underway to clarify the formation mechanisms for this interesting group of biological crystals.

Combining structure- and pigment-based coloration is a common strategy used in organisms to produce a variety of optical effects, such as butterflies and blue-rayed limpets [56]. The combination of pigments and guanine crystals (usually matte) has also been reported earlier in some spider species. For example, ommochrome pigment granules and matte guanine crystals produce bright yellow colour and white reflectance in the spider of *Misumena vatia* [14,40]. In addition to using the pigments and guanine crystals in different locations, we observed that the microsphere-shaped pigments and guanine microplates are co-localized with the reflective guanine crystals beneath the pigmented microspheres in *P. rubroargentea*. As shown by the microspectrometry measurements, this organization increases the absorption and fluorescence efficiency of the microspheres, allowing for very strong red coloration with a small amount of material (usually one or two layers of microspheres are observed). The red fluorescence is very stable and did not show significant photo bleaching. However, due to the localized distribution and small quantity, we were not able to identify the chemical composition of the red microspheres. We suspect that the layered microspheres serve as scaffold for loading the as of yet unidentified red fluorophores.

Similar to other arthropods, spiders have protective cuticular exoskeletons covering their bodies made of a stiff material called cuticle. In general, the cuticle provides structural support for the animal's body, by covering the entire surface and protecting it from dessication [57,58], as well as invaginating into the body to create attachment points for muscles [59]. The main building block of arthropod cuticle is chitin [60], in the form of laminated composite material comprised chitinous microfibrils in a proteinous matrix [61–63]. It has been shown that, depending on the types, amount, and cross-linking density of proteins in the matrix, chitin layering orientation, hydration and other factors, the structure and mechanical properties (such as rigidity) of a spider's cuticle can vary in different parts of the spider's body. For example, to accommodate the great volumetric changes associated with spiders' sporadic feeding [64] as well as developing eggs in females, the cuticular layering in

spiders' abdomens is typically more elastic and thinner compared with other parts of the body [61,65].

In this work, the cuticular layer of the *P. rubroargentea* body has also been shown to vary considerably in different regions of the spider's body for optical purposes. Observations made from TEM, transmission optical images and confocal imaging demonstrate that the cuticle is very homogeneous and transparent where the guanine crystals are located; however, in the red region, the cuticle appears to be divided into two sublayers, with the bottom sublayer appearing to be tanned or pigmented. Moreover, the *Phoroncidia* species we have examined have a 'hard-bodied' abdomen with patterned coloration, whereas other theridiids such as *T. emertoni* have a 'softer' abdomen.

The red coloration can be retained for decades in ethanol-preserved specimens; however, in some instances, we observed that mechanical disruption of the exoskeleton in this species can result in a loss of this red pigmentation (electronic supplementary material, figure S8D, E). These results are significant and suggest that the combined effect of thick and heavily sclerotized exoskeleton, the armouring of the twinned guanine crystals, and the chambered pigment-containing microspheres, creates a composite architecture that protects the red pigment from chemical attack and subsequent bleaching. While there are other cases of environmentally protected pigment encapsulation in biological systems, such as in the calcareous skeletal elements of the gorgonians, which can retain their pigment even when preserved in ethanol for over a century (J. C. Weaver and S. J. Kariko, personal observations), the case reported here for *P. rubroargentea* represents the first documented case of this phenomenon in an entirely organic system. Despite the advancement of knowledge provided by the present work, further research on *Phoroncidia* cuticle is needed to better understand its unique properties (as well as the chemical composition of the pigments in each species) and how this contributes to overall colour producing strategies.

Our understanding of how and why colour has evolved in spiders is limited. As stated by Taylor and McGraw, the body colorations of spiders may serve as a way of communicating information about themselves, such as their age, sex, mate quality and fighting ability, to other individuals [66]. Conspicuous coloration can also be a warning signal to predators [67] – common warning colour combinations include yellow, red and black [66]. Bright markings on spiders based on guanine materials are hypothesized as functions of camouflage, attraction of prey, intimidation of predators or for UV protection [22]. Since many prey items (insects) and predators (birds and insects) of spiders have very good vision that extends well into the UV range, it could be that bright colours have evolved for communicating with predators for attracting prey or for crypsis [38,39]. With findings of the widespread distribution of fluorescence in spiders, it is likely that fluorescence serves an important function.

Although *Phoroncidia* first appeared in the arachnological literature in the late 1880s, we have learned little about its natural history and behaviour, which also limits the interpretation of the observed multi-coloration pattern in *Phoroncidia* for this work. Knowledge of the natural history of *Phoroncidia* is limited to habitat notes such as: 'found in bushes' [68], 'on sandhills' [69], at 1300 m in 'very wet subtropical forest' [70]; trees [71]; 'in pitfall traps in floodplain deciduous forests' [72]; 'on Spanish moss' [73]; 'on a single line of silk near the river' [50]; and 'in copal from Madagascar' [74].

Despite the lack of behavioural data, there are several possibilities as to why *P. rubroargentea* may possess its unique coloration. The red/black combination of colours may serve as a warning coloration, similar to ladybugs [75]. Oxford and Gillespie argue that it is metabolically costly to produce colour pigments, yet it is maintained by predators hunting by sight such as birds and wasps [26] and in Madagascar, possibly chameleons. Having a thin layer of pigment reflected by a mirror-layer could be one way to produce and maintain vibrant colour efficiently in an environment filled with sight-hunting predators. While this may be metabolically costly, if it is advantageous to be red for defensive/warning purposes, then it could be worth the extra expense of maintaining the mirror layer of guanine versus eliminating it as waste product.

Moreover, as the bodies of spiders get smaller, thermal and hydration regulation becomes more critical due to a larger surface-area-to-volume ratio. It has been hypothesized that silver guanine could be useful in regulating these by altering surface albedo [26]. Oxford found that the presence of guanine tends to be greater in species living in more exposed 'open' environments [21]. Some specimens used for this study were collected near the river where the sunlight and exposure is greater than in the dappled light of the rainforest, lending support to this hypothesis.

In addition to interspecies communication, thermal regulation and UV protection, the complex colour pattern observed in *P. rubroargentea* may also serve for intraspecies communication. This hypothesis is supported by the observation that their eye morphology (different sizes and sometimes elevated) is unique among the theridiid species (with eyes of relatively similar size arranged in two rows), who usually have poor vision. *Phoroncidia* species of Madagascar have larger medial eyes similar to the eye pattern of other groups with good vision like salticids and lycosids. Also, *Phoroncidia* have their eight eyes elevated on a turret, and in the case of some males like *P. ambatolahy*, the eyes are elevated on a neck-like structure. Further investigation on the visual acuity of *P. rubroargentea* might lead to more insights for this hypothesis. Moreover, another observation also suggests the possibility of intraspecies communication based on the optical appearance of Phoroncidia. We currently study another species of *Phoroncidia* with similar coloration (shimmery red, silver and black, ornamented with four black spines) to *P. rubroargentea*, but unlike *P. rubroargentea* which is often found with a line of guanine crystals underscoring the epigastric furrow below the female epigynum (or genitalia), this species has a large, shimmery, rectangular patch of guanine in a similar location under the female's epigynum. It is possible this could be used for attracting and/or guiding mates as four of the five female specimens being examined have what could be mating plugs (which would suggest evidence of sperm competition/male–male competition).

The strong red fluorescence resulting from the microspheres requires a particular discussion. Fluorophores occur widely in Nature and have been found in a diversity of marine animals such as fishes, mantis shrimp and jellyfish [76–78], but less so among terrestrial animals, where some parrots [79], insects [80], arachnids [40] and frogs [81] have been found to fluoresce. Several hypotheses have been proposed to explain fluorescence in spiders and scorpions: as a sunscreen to protect from ultraviolet light [12]; camouflage

[82,83]; prey attraction [14] and sexual signalling [84]. Brandt & Masta [40] have found that the expression of fluorescence differs between the sexes as well as changes across the life stages of the crab spider *M. vatia*. In the case of *P. rubroargentea*, the red fluorescence results from the microscopic structures positioned in specific regions of the body, as opposed to the green fluorescence from the overall spider body without location specification as in the case of scorpions. It is, therefore, thus likely that the red fluorescence resulting from the microspheres is biologically functional, with potentially multiple overlapping functions from UV protection, to attracting prey items, to crypsis and interspecies communication.

Data accessibility. Electronic supplementary material (additional structural analysis and optical measurement) is available online.

Authors' contributions. S.J.K. and J.C.W. conceived the study. L.Li, M.K. and S.J.K. designed and supervised the project. C.M., S.J.K. and L.Li embedded the specimen and performed microtoming to obtain thin slices for both optical and electron microscopic analysis. C.M., J.C.W. and L.Li acquired SEM images. C.M. and L.Li acquired TEM images. L.Li conducted SAED measurements. D.G., L.Leiserowitz, and L.Li performed SAED data analysis. J.V.I.T. conducted and processed confocal and fluorescent measurements with specimen handling by S.J.K. M. K. performed microspectrometry measurements with S.J.K. handling specimens. All authors interpreted results. L.Li and S.J.K. prepared figures, tables, and movies and wrote draft manuscript. All authors revised manuscript for submission.

Competing interests. We declare we have no competing interests.

Funding. J.V.I.T. was supported by the European Commission through the Seventh Framework Programme (FP7) project DynaSLIPS (project no. 626954). M.K. was support by the National Science Foundation through the 'Designing Materials to Revolutionize and Engineer our Future' program (DMREF-1533985). The field research was generously supported by the Fulbright Commission, an Isabella Briggs Travelling Fellowship, Harvard Travelers Club, Douroncouli Foundation and the Museum of Comparative Zoology; expeditions supported by Patagonia, The North Face, Leatherman, York Pack, Easter Seals Headlamps and Timex. Additional expedition support provided by the Institute for the Conservation of Nature. This work was performed in part at the Center for Nanoscale Systems (CNS), a member of the National Nanotechnology Coordinated Infrastructure Network (NNCI), which is supported by the National Science Foundation under NSF award no. 1541959. CNS is part of Harvard University.

Acknowledgements. This paper is dedicated to Herbert W. Levi (who passed away during the course of this research) in honour of his early work on *Phoroncidia* and for mentoring S.J.K. We would like to extend special recognition and thanks to Telo Albert who worked with S.J.K. at Vatoharanana and whose fieldwork was invaluable on several expeditions that resulted in finding the spiders that inspired this study.

We thank the government and people of Madagascar, Madagascar Ministry of Forests, Environment and Tourism/ Direction des Eaux et Forêts of the Ministre d' Etat a L'Agriculture et au Development Rural, the CAFF/CORE oversight committee, the accord of collaboration with Duke University, Ministry of Higher Education and the Department of Water and Forests, and Madagascar National Parks (ANGAP) for making our work in Madagascar possible as well as the arachnofauna.

We are grateful for vital logistical and infrastructural support from Madagascar Institut pour la Conservation des Ecosystèmes Tropicaux (MICET), particularly director Benjamin Andriamihaja; and to Centre ValBio, especially Eileen Larney with John Cadle and support personnel. Thanks also to Berthe Rakotosamimanana and Celestine Ravaorinorma for assistance with permits. Thanks to Patricia Wright and Patricia Paladines at the Institute for the Conservation of Tropical Environments (ICTE) and Noel Rowe for vital field and logistical support.

Thanks to the RNP research technicians/guides: Emile Rajeriarison, Loret Rasabo, the late Georges Rakotonirina, the late Talata Pierre; and the late Zafy Albert, guardian of Vato: this work would not have been possible without all of you. We acknowledge assistance in the field by Barbara and the late Vince Roth; thanks to Andy Kingman for early fieldwork. Thanks to the team that attempted with robust effort and little luck to find additional *P. rubroargentea* spiders in Madagascar: William Montag, Telo Albert, and Rahanitriniaina Sahondra Lalao. Also, thanks to Bettina Lengsfeld for sewing special beating sheets and Paul Bertner for use of his field photos. Thanks to Dan Rossman for technical support.

Specimens from SJK expeditions were collected under permit no. 017-MEF/DEF/SDN/FFE/AUT from the Ministere des Eaux et Forets of Madagascar.

We gratefully acknowledge the Museum of Comparative Zoology's Invertebrate Zoology collections for support: Professor Gonzalo Giribet; Adam Baldinger and Laura Leibensperger, Jennifer Lenihan Trimble and Penny Benson as well as the Ernst Mayr Library staff especially Connie Rinaldo, Robert Young, Mary Sears, Dorothy Barr, April Collins, Ronnie Broadfoot and Dana Fisher. Thanks to Curators Charles Griswold and Lauren Esposito as well as Darrell Ubick and Anthea Carmichael for loaning specimens from the California Academy of Sciences as well as the many curators who assisted with collections searches for *Phoroncidia* specimens or provided helpful information: Janet Beccaloni, Rudy Jocqué and Didier Van den Spiegel, Zoe Simmons, Karin Sindemark Kronestedt and Elin Sigvaldadottir, Norman Platnick and Louis Sorkin. Thanks to Curator Christine Rollard for her assistance at the Museum National D'Historie Naturelle, Paris. Thanks to Adam Graham and the team at Harvard's Center for Nanoscale Systems. L.L. thanks the Department of Mechanical Engineering at Virginia Tech for support.

Thanks to four anonymous reviewers whose comments improved this manuscript.

References

1. Hooke R. 1665 *Micrographia*. London, UK: Royal Society.
2. Newton I, Sarton G. 1930 Discovery of the dispersion of light and of the nature of color (1672). *Isis* **14**, 326–341. (doi:10.1086/346510)
3. Prum RO. 2006 Anatomy, physics, and evolution of structural colors. In *Bird coloration, volume 1 mechanisms and measurements* (eds GE Hill, KJ McGraw), pp. 295–353. Cambridge, MA: Harvard University Press.
4. Stoddard MC, Prum RO. 2011 How colorful are birds? Evolution of the avian plumage color gamut. *Behav. Ecol.* **22**, 1042–1052. (doi:10.1093/beheco/arr088)
5. Seago AE, Brady P, Vigneron J-P, Schultz TD. 2009 Gold bugs and beyond: a review of iridescence and structural colour mechanisms in beetles (Coleoptera). *J. R. Soc. Interface* **6**, S165–S184. (doi:10.1098/rsif.2008.0354.focus)
6. Srinivasarao M. 1999 Nano-optics in the biological world: beetles, butterflies, birds, and moths. *Chem. Rev.* **99**, 1935–1962. (doi:10.1021/cr970080y)
7. Vukusic P, Sambles JR, Lawrence CR, Wootton RJ. 1999 Quantified interference and diffraction in single morpho butterfly scales. *Proc. R. Soc. B* **266**, 1403–1411. (doi:10.1098/rspb.1999.0794)
8. Vukusic P, Sambles JR, Lawrence CR. 2000 Structural colour: colour mixing in wing scales of a butterfly. *Nature* **404**, 457. (doi:10.1038/35006561)
9. Parker AR, Hegedus Z. 2003 Diffractive optics in spiders. *J. Opt. A* **5**, S111. (doi:10.1088/1464-4258/5/4/364)
10. Foelix RF. 1982 *Biology of spiders*. Cambridge, MA: Harvard University Press.
11. Hsiung B-K, Siddique RH, Jiang L, Liu Y, Lu Y, Shawkey MD, Blackledge TA. 2017 Tarantula-inspired noniridescent photonics with long-range order. *Adv. Opt. Mater.* **5**, 1600599. (doi:10.1002/adom.201600599)

12. Hsiung B-K, Blackledge TA, Shawkey MD. 2014 Structural color and its interaction with other color-producing elements: perspectives from spiders. In *Proc. SPIE 9187, The Nature of Light: Light in Nature V, San Diego, CA, 17–21 August*. 91870B. Bellingham, WA: SPIE.
13. Insausti TC, Casas J. 2008 The functional morphology of color changing in a spider: development of ommochrome pigment granules. *J. Exp. Biol.* **211**, 780–789. (doi:10.1242/jeb.014043)
14. Théry M, Casas J. 2009 The multiple disguises of spiders: web colour and decorations, body colour and movement. *Phil. Trans. R. Soc. B* **364**, 471–480. (doi:10.1098/rstb.2008.0212)
15. Seligy VL. 1972 Ommochrome pigments of spiders. *Comp. Biochem. Physiol. A* **42**, 699–709. (doi:10.1016/0300-9629(72)90448-3)
16. Wunderlin J, Kropf C. 2013 'Rapid Colour Change in Spiders'. In *Spider ecophysiology* (ed. W Nentwig), pp. 361–370. Berlin, Germany: Springer.
17. Graf B, Nentwig W. 2001 Ontogenetic change in coloration and web-building behavior in the tropical spider *Eriophora fuliginea* (Araneae, Araneidae). *J. Arachnol.* **29**, 104–110. (doi:10.1636/0161-8202(2001)029[0104:OCICAW]2.0.CO;2)
18. Drake N. 2016 Disco spider pulsates with color, baffling scientists. *Natl Geogr. Soc.* (https://news.nationalgeographic.com/2016/12/spiders-pulating-mystery-singapore)
19. Dumanli AG, Kamita G, Landman J, van der Kooij H, Glover, BJ, Baumberg, JJ, Steiner U, Vignolini S. 2014 Controlled, bio-inspired self-assembly of cellulose-based chiral reflectors. *Adv. Opt. Mater.* **2**, 646–650. (doi:10.1002/adom.201400112)
20. Millot J. 1926 Contribution A l'histophysiologie des Aranides. *Bull. Biol. Ft. Belg. Suppl.* VIII.
21. Oxford G. 1997 Guanine as a colorant in spiders: development, genetics, phylogenetics and ecology. In *Proc. 17th Eur. Colloq. Arachnol. Edinburgh, UK, 14–18 July*, pp. 121–131. British Arachnological Society.
22. Levy-Lior A, Shimoni E, Schwartz O, Gavish-Regev E, Oron D, Oxford G, Weiner S, Addadi L. 2010 Guanine-based biogenic photonic-crystal arrays in fish and spiders. *Adv. Funct. Mater.* **20**, 320–329. (doi:10.1002/adfm.200901437)
23. Nentwig W. 1987 *Ecophysiology of spiders*. Berlin, Germany: Springer.
24. Stavenga DG, Otto JC, Wilts BD. 2016 Splendid coloration of the peacock spider. *J. R. Soc. Interface* **13**, 20160437. (doi:10.1098/rsif.2016.0437)
25. Holl A. 1987 Coloration and Chromes. In *Ecophysiology of spiders* (ed. W Nentwig), pp. 16–25. Berlin, Germany: Springer.
26. Oxford GS, Gillespie RG. 1998 Evolution and ecology of spider coloration. *Annu. Rev. Entomol.* **43**, 619–643. (doi:10.1146/annurev.ento.43.1.619)
27. Oxford GS, Gillespie RG. 2001 Portraits of evolution: studies of coloration in Hawaiian spiders the discrete color polymorphisms in spiders allow the study of evolution 'in action'. *BioScience* **51**, 521–528. (doi:10.1641/0006-3568(2001)051[0521:POESOC]2.0.CO;2)
28. Croucher PJ, Brewer MS, Winchell CJ, Oxford GS, Gillespie RG. 2013 De novo characterization of the gene-rich transcriptomes of two color-polymorphic spiders, *Theridion grallator* and *T. californicum* (Araneae: Theridiidae), with special reference to pigment genes. *BMC Genomics* **14**, 862. (doi:10.1186/1471-2164-14-862)
29. Seligy VL. 1969 Biochemical aspects of pigment variation in the spider *Enoplognatha ovata* (Clerck) (Araneae: Theridiidae). *Can. J. Zool.* **47**, 1103–1105. (doi:10.1139/z69-173)
30. Riddle O. 1909 Our knowledge of melanin color formation and its bearing on the mendelian description of heredity. *Biol. Bull.* **16**, 316–351. (doi:10.2307/1536192)
31. Hsiung B-K, Blackledge TA, Shawkey MD. 2015 Spiders do have melanin after all. *J. Exp. Biol.* **218**, 3632–3635. (doi:10.1242/jeb.128801)
32. Holl A, Wudiger WM. 1975 A new biliverdin conjugate in the spider, Micromata rosea (Sparassidae). *J. Comp. Physiol. B Biochem. Syst. Environ. Physiol.* **98**, 189–191. (doi:10.1007/BF00706130)
33. Goodwin TW. 1980 *The biochemistry of the carotenoids: volume I plants*. Dordrecht, the Netherlands: Springer.
34. Lintig J, Welsch R, Bonk M, Giuliano G, Batschauer A, Kleinig H. 1997 Light-dependent regulation of carotenoid biosynthesis occurs at the level of phytoene synthase expression and is mediated by phytochrome in *Sinapis alba* and *Arabidopsis thaliana* seedlings. *Plant J.* **12**, 625–634. (doi:10.1046/j.1365-313X.1997.00625.x)
35. Lawrence RF. 1954 Fluorescence in Arthropoda. *J. Entomol. Soc. Southern Africa* **17**, 167–170.
36. Kloock CT, Kubli A, Reynolds R. 2010 Ultraviolet light detection: a function of scorpion fluorescence. *J. Arachnol.* **38**, 441–445. (doi:10.1636/B09-111.1)
37. Stachel SJ, Stockwell SA, Van Vranken DL. 1999 The fluorescence of scorpions and cataractogenesis. *Chem. Biol.* **6**, 531–539. (doi:10.1016/S1074-5521(99)80085-4)
38. Andrews K, Reed SM, Masta SE. 2007 Spiders fluoresce variably across many taxa. *Biol. Lett.* **3**, 265–267. (doi:10.1098/rsbl.2007.0016)
39. Brandt E. 2012 Externally-Expressed Fluorescence across Sexes, Life Stages, and Species of Spiders. MS thesis, Portland State University, Portland, OR.
40. Brandt EE, Masta SE. 2017 Females are the brighter sex: differences in external fluorescence across sexes and life stages of a crab spider. *PLOS ONE* **12**, e0175667. (doi:10.1371/journal.pone.0175667)
41. World Spider Catalog. (18.5, Version). 2017 *Natural History Museum*. See http://wsc.nmbe.ch.
42. Foelix R, Rast B, Erb B. 2009 Palpal urticating hairs in the tarantula *Ephebopus*: fine structure and mechanism of release. *J. Arachnol.* **37**, 292–298. (doi:10.1636/sh08-106.1)
43. Ingram AL, Ball AD, Parker AR, Deparis O, Boulenguez J, Berthier S. 2009 Characterization of the green iridescence on the chelicerae of the tube web spider, *Segestria florentina* (Rossi 1790) (Araneae, Segestriidae). *J. Arachnol.* **37**, 68–71. (doi:10.1636/SH07-87.1)
44. Ingram AL, Deparis O, Boulenguez J, Kennaway G, Berthier S, Parker AR. 2011 Structural origin of the green iridescence on the chelicerae of the red-backed jumping spider, *Phidippus johnsoni* (Salticidae: Araneae). *Arthropod. Struct. Dev.* **40**, 21–25. (doi:10.1016/j.asd.2010.07.006)
45. Hsiung B-K, Deheyn DD, Shawkey MD, Blackledge TA. 2015 Blue reflectance in tarantulas is evolutionarily conserved despite nanostructural diversity. *Sci. Adv.* **1**, 1500709. (doi:10.1126/sciadv.1500709)
46. Berland L. 1913 Descriptions de deux espèces nouvelles d'arachnides africaines du genre *Phoroncidia* Westwood (Araneae Theridiidae). *Bull. Mus. Paris* **1913**, 75–78.
47. Arnedo MA, Coddington J, Agnarsson I, Gillespie RG. 2004 From a comb to a tree: phylogenetic relationships of the comb-footed spiders (Araneae, Theridiidae) inferred from nuclear and mitochondrial genes. *Mol. Phylogenet. Evol.* **31**, 225–245. (doi:10.1016/S1055-7903(03)00261-6)
48. Agnarsson I. 2004 Morphological phylogeny of cobweb spiders and their relatives (Araneae, Araneoidea, Theridiidae). *Zool. J. Linn. Soc.* **141**, 447–626. (doi:10.1111/j.1096-3642.2004.00120.x)
49. Liu J, May-Collado LJ, Pekár S, Agnarsson I. 2016 A revised and dated phylogeny of cobweb spiders (Araneae, Araneoidea, Theridiidae): a predatory Cretaceous lineage diversifying in the era of the ants (Hymenoptera, Formicidae). *Mol. Phylogen. Evol.* **94**, 658–675. (doi:10.1016/j.ympev.2015.09.023)
50. Kariko SJ. 2014 The Glitterati: four new species of *Phoroncidia* (Araneae: Theridiidae) from Madagascar, with the first description of the male of *P. aurata* O. Pickard—Cambridge, 1877. *Arachnol.* **16**, 195–213. (doi:10.13156/arac.2014.16.6.195)
51. Levi HW, Randolph DE. 1964 A key and checklist of American spiders of the family Theridiidae North of Mexico (Araneae). *J. Arachnol.* **3**, 31–51.
52. Thewalt U, Bugg CE, Marsh RE. 1971 The crystal structure of guanine monohydrate. *Acta Crystallogr. B* **27**, 2358–2363. (doi:10.1107/S0567740871005880)
53. Guille K, Clegg W. 2006 Anhydrous guanine: a synchrotron study. *Acta Crystallogr. Sect. C: Cryst. Struct. Commun.* **62**, 515–517. (doi:10.1107/S0108270106026011)
54. Hirsch A, Palmer BA, Elad N, Gur D, Weiner S, Addadi L, Kronik L, Leiserowitz L. 2017 Biologically controlled morphology and twinning in guanine crystals. *Angew. Chem. Int. Ed.* **56**, 9420–9424. (doi:10.1002/anie.201704801)
55. Gur D, Palmer BA, Weiner S, Addadi L. 2017 Light manipulation by guanine crystals in organisms: biogenic scatterers, mirrors, multilayer reflectors and photonic crystals. *Adv. Funct. Mater.* **27**, 1603514. (doi:10.1002/adfm.201603514)

56. Li L, Kolle S, Weaver JC, Ortiz C, Aizenberg J, Kolle M. 2015 A highly conspicuous mineralized composite photonic architecture in the translucent shell of the blue-rayed limpet. *Nat. Commun.* **6**, 6322. (doi:10.1038/ncomms7322)
57. Nemenz H. 1954 Über den Wasserhaushalt einiger Spinnen. *Öst. Zool. Z* **5**, 123–158.
58. Nemenz H. 1955 *Über den Bau der Kutikula und dessen Einflu auf die Wasserabgabe bei Spinnen*. Berlin, Germany: Springer.
59. Bitsch C, Bitsch J. 2005 Evolution of eye structure and arthropod phylogeny. In *Crustaceans and arthropod relationships* (ed. S Koenemann). Boca Raton, FL: Taylor and Francis.
60. Fusenig NE. 1986 Mammalian epidermal cells in culture. In *Biology of the integument II, vertebrates* (eds J Bereiter-Hahn, AG Matoltsy, KS Richards), pp. 409–442. Berlin, Germany: Springer.
61. Barth FG. 1973 Microfiber reinforcement of an arthropod cuticle. *Z. Zellforsch* **144**, 409–433. (doi:10.1007/BF00307585)
62. Rudall K. 1963 The chitin/protein complexes of insect cuticles. *Adv. Insect Physiol.* **1**, 257–313. (doi:10.1016/S0065-2806(08)60177-0)
63. Neville AC, Parry DA, Woodhead-Galloway J. 1976 The chitin crystallite in arthropod cuticle. *J. Cell Sci.* **21**, 73–82.
64. Slansky, Frank, Rodriguez JG. 1986 *Nutritional ecology of insects, mites, spiders and related invertebrates*. New York, NY: Wiley.
65. Dalingwater JE. 1987 'Chelicerate cuticle structure'. In *Ecophysiology of spiders* (eds W Nentwig), pp. 3–15. Berlin, Germany: Springer.
66. Taylor LA, McGraw KJ. 2007 Animal coloration: sexy spider scales. *Curr. Biol.* **17**, R592–R593. (doi:10.1016/j.cub.2007.05.064)
67. Marples NM, Kelly DJ, Thomas RJ, Harrison R. 2005 Perspective: the evolution of warning coloration is not paradoxical. *Evol.* **59**, 933–940. (doi:10.1554/04-448)
68. Emerton JH. 1882 New England spiders of the family Theridide. Theridiidae. Trans. Conn. Acad. 6.
69. Marples, JB. 1995 A new type of web spun by spiders of the genus *Ulesanis* with the description of two new species. *Proc. Zool. Soc. Lond.* **125**, 751–760. (doi:10.1111/j.1096-3642.1995.tb00625.x)
70. Eberhard WG. 1981 The single line web of *Phoroncidia studo* Levi (Araneae: Theridiidae): a prey attractant? *J. Arachnol.* **9**, 229–232.
71. Edwards RL, Edwards EH. 1997 Behavior and niche selection by mailbox spiders. *J. Arachnol.* **25**, 20–30.
72. Draney ML. 1997 Ground-layer spiders (Araneae) of a Georgia piedmont floodplain agroecosystem: species list, phenology and habitat selection. *J. Arachnol.* **25**, 333–351.
73. Frank JH *et al.* 2004 Invertebrate animals extracted from native Tillandsia (Bromeliales: Bromeliaceae) in Sarasota county, Florida. *Florida Entomol.* **87**, 176–185. (doi:10.1653/0015-4040(2004)087[0176:IAEFNT]2.0.CO;2)
74. Wunderlich J. 2004 Fossil spiders in amber and copal.
75. DolenskÁ M, NedvĚD O, VeselÝ P, TesaŘOvÁ M, Fuchs R. 2009 What constitutes optical warning signals of ladybirds (Coleoptera: Coccinellidae) towards bird predators: colour, pattern or general look? *Biol. J. Linn. Soc.* **98**, 234–242. (doi:10.1111/j.1095-8312.2009.01277.x)
76. Harant UK, Michiels NK, Anthes N, Meadows MG. 2016 The consistent difference in red fluorescence in fishes across a 15 m depth gradient is triggered by ambient brightness, not by ambient spectrum. *BMC Res. Notes* **9**, 107. (doi:10.1186/s13104-016-1911-z)
77. Mazel CH, Cronin TW, Caldwell RL, Marshall NJ. 2004 Fluorescent enhancement of signaling in a mantis shrimp. *Science* **303**, 51. (doi:10.1126/science.1089803)
78. Voss U, Larrieu A, Wells DM. 2013 From jellyfish to biosensors: the use of fluorescent proteins in plants. *Int. J. Dev. Biol.* **57**, 525–533. (doi:10.1387/ijdb.130208dw)
79. Arnold KE, Owens IPF, Marshall NJ. 2002 Fluorescent signaling in parrots. *Science* **295**, 92. (doi:10.1126/science.295.5552.92)
80. Wiesenborn WD. 2011 UV-excited fluorescence on riparian insects except hymenoptera is associated with nitrogen content. *Psyche. J. Entomol.* **2011**, Article ID 875250. (doi:10.1155/2011/875250)
81. Taboada C *et al.* 2017 Naturally occurring fluorescence in frogs. *Proc. Natl Acad. Sci. USA* **114**, 3672–3677. (doi:10.1073/pnas.1701053114)
82. Théry M, Casas J. 2002 Visual systems: predator and prey views of spider camouflage. *Nature* **415**, 133. (doi:10.1038/415133a)
83. Théry M, Debut M, Gomez D, Casas J. 2005 Specific color sensitivities of prey and predator explain camouflage in different visual systems. *Behav. Ecol.* **16**, 25–29. (doi:10.1093/beheco/arh130)
84. Lim MLM, Land MF, Li D. 2007 Sex-specific UV and fluorescence signals in jumping spiders. *Science* **315**, 481. (doi:10.1126/science.1134254)